Science of Sintering, **49** (2017) 455-467

doi: https://doi.org/10.2298/SOS1704455L

UDK: 621.926.087, 622.785

Characterisation of $Mn_{0.63}Zn_{0.37}Fe_2O_4$ Powders After Intensive Milling and Subsequent Thermal Treatment

Nebojša Labus[1*], Zorka Vasiljević[1], Obrad Aleksić[1], Miloljub Luković[1], Smilja Marković[1], Vladimir Pavlović[1], Slavko Mentus[2,3], Maria Vesna Nikolić[4]

[1]Institute of Technical Sciences of SASA, Knez Mihailova 35, 11000 Beograd, Serbia
[2]Faculty of Physical Chemistry, Studenski trg 12-16, 11158 Belgrade, University of Belgrade, Serbia
[3]Serbian Academy of Sciences and Arts, Knez Mihailova 35, 11000 Belgrade, Serbia
[4]Institute for Multidisciplinary Research, University of Belgrade, Kneza Višeslava 1, 11000 Beograd, Serbia

Abstract:

Commercial Mn-Zn powder ($Mn_{0.63}Zn_{0.37}Fe_2O_4$, 93 wt. % and Fe_2O_3 7 wt. %) was milled 0.5, 1, 2 and 4 hours in a planetary ball mill. The goal was to observe intensive milling influences on oxidation and reduction processes that will happen during subsequent heating. Powders were characterized with XRD, SEM and particle seizer. Subsequent heating was monitored on TGA/DTA in an air atmosphere. After compaction of the milled powders, sintering was also performed in a dilatometric device. Sintered specimens were characterized micro structurally with SEM on a fresh breakage. Obtained differential TGA diagrams suggest intensive changes during prolonged milling of the oxidation kinetics on heating. Ferrite powders changed with milling as well as with second run heating were characterized to enable determination of the potentially best ratio of milling and heating to be applied to obtain the desired microstructure.

Keywords*: Ferrites; Milling; Sintering; Dilatometry.*

1. Introduction

The complexity of the Mn-Zn ferrite system is obvious due to the fact, that basic oxide Fe_3O_4 is one of the most investigated systems [1]. Complexity arises from the spinel structure that can be inverse, normal and random, where at constant total pressure all spinels randomize to the same extent. Furthermore, two types of non-stoichiometry, positive and negative occur due to cation vacancies and cation interstitials as major defects. Also, electrostatic equilibrium with the electrostatic interaction between charged defects due to redox equilibrium between $Fe^{2+}$and Fe^{3+} can become significant at higher defects concentrations. Furthermore, iron-based spinel solid solutions where the iron cation is replaced with other cations has opened the varying parameters possibilities to a large extent. Even with the fact, that cation vacancies and cation interstitials are the majority defects, oxygen content with oxygen activity is unknown as well as the cation defects locations of different substituted species [2]. Also, if the cations are substituted, then the mobility of

*) **Corresponding author:** nebojsa.labus@itn.sanu.ac.rs

individual species is changed [3]. If the overall concentrations of the substituted species are large enough, the reactions of phase formation are possible [4]. Another parameter important for this investigation is mechanical treatment [5, 6] that enables different types of polycrystalline structures during subsequent heating [7]. All these physical and chemical influences during synthesis of the ferrite compound finally govern the most important consequence - the properties [8].

This mostly refers to magnetic properties, although Mn-Zn ferrite has electric permeability and specific electric resistivity, higher than existing metallic alternatives at high frequencies up to 1 MHz [9]. This work is trying to connect mechanical treatment of Mn-Zn ferrite powder with subsequent behavior during heating. Namely, the usual mechanochemical procedure lasts shorter and prolonged milling leads to the unknown concentration gradients of Mn ions due to possible mechanochemical reactions and also to the formation of Kirkendall pores due to counter diffusion of the ions with different diffusivities [10]. These changes are, besides microstructure changes, clearly visible on the reaction kinetics monitored on TGA/DTA diagrams. So, eventual further investigations would lead to a determination of the optimal extent of milling and heating proportions and thus to the desired composition and structure.

2. Experimental

Commercial Mn-Zn ferrite powder (composition $Mn_{0.63}Zn_{0.37}Fe_2O_4$, 93 wt.% and Fe_2O_3 7 wt.%) was milled in a planetary ball mill for 30, 60, 120 and 240 minutes. The Fritsch pulverisette 4 planetary ball mill with 780 revolutions in a minute and ball to powder ratio 20 to 1 was used. Balls were 10 mm in diameter made of stainless steel. XRD analysis of the starting and milled powders was performed on a Philips PW1050 diffractometer with CuK_α radiation, step 0.02s hold time 10s. Structural refinement was carried out by the Rietveld method using the GSAS package [11] with the EXPGUI graphical user interface [12]. SEM micrographs of the activated powders were recorded on a TESCAN Electron microscope VEGA TS 5130MM device while sintered specimens on breakage were monitored on a JEOL JSM 6390 LV device. The average size and particle size distribution in a water powder suspension were determined by a Mastersizer 2000 (Hydro 2000S sample dispersion unit) Malvern Instruments Ltd., UK laser particle size analyzer (PSA) covering the particle size range of 0.02–2000 μm with previous treatment in an ultrasonic bath for 5 min. Compaction was conducted with an applied uniaxial pressure of 200 MPa on both sides without binder and lubricant. Green disc samples were sintered in the air within the temperature interval 800 -1300^{o}C for 2 hours in a chamber furnace. Sample density was determined by dimension measurements. Sintering was also performed in a tubular furnace in the Baehr 802 s dilatometric device. The applied heating rate was 10^{o}C/min, up to 1300^{o}C, with a holding time of 10 minutes and controlled cooling 10^{o}C/min. Differential thermal analysis with thermal gravimetry (TGA/DTA) were carried out simultaneously using a SDT 2960 thermo balance TA instrument. The heating rate was 15^{o}C/min up to 1200^{o}C.

3. Results and discussion

XRD of the starting powder as expected showed peaks for $MnZnFe_2O_4$ and Fe_2O_3 (hematite), Fig. 1. The estimated composition of the starting powder was$Mn_{0.63}Zn_{0.37}Fe_2O_4$ 93 wt.%, Fe_2O_3 7 wt.%. According to X-ray analysis, the composition during milling remains unchanged.

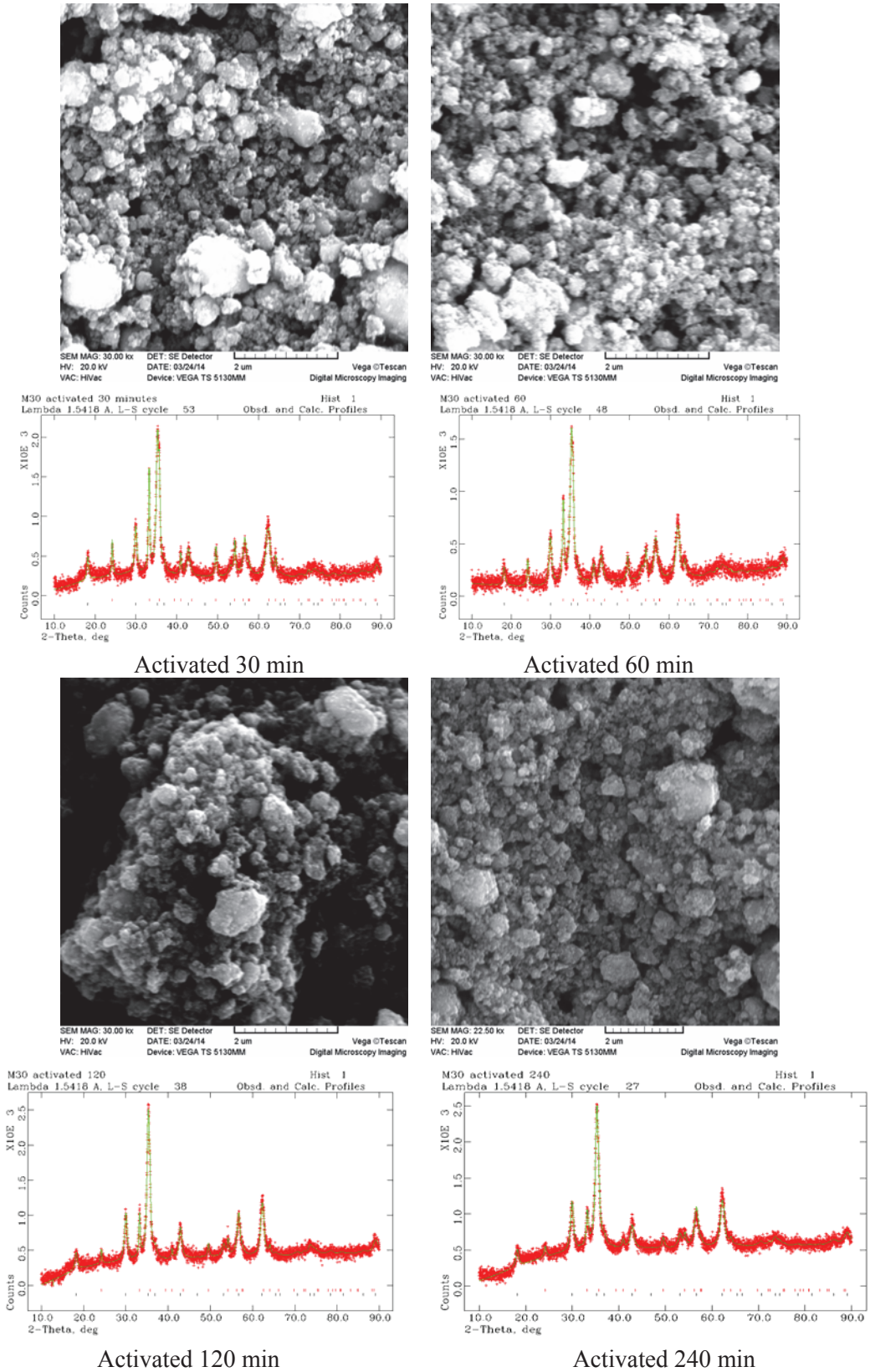

Fig. 1. Scanning electron micrographs and refined XRD patterns of the powders milled 30, 60, 120 and 240 minutes.

SEM micrographs of the activated powders, Fig. 1, show that agglomeration is very noticeable with the largest agglomerates in the 120 minutes milled powder. It was not possible to note differences in powder particle size of activated powders from SEM micrographs. Judging from the results of Rietveld analysis, the crystallite size is diminishing until 60 minutes and afterward for longer activation periods is almost constant. The mechanical activation process consists of two agglomeration processes. Primary agglomeration is common for powders and it originates from weak interactions between particles. Particle size reduction in the beginning of the milling process is specific and with these milling conditions, it is usually finished in the very beginning. It is not detected here as the lowest observed milling time was 30 minutes. Secondary agglomeration occurs after an intensive process of milling and represents cold welding of the particles. Agglomeration visible on the powders activated 30 minutes is subscribed to a secondary agglomeration process. Intensive milling is affecting the crystallite structure. The maximal strain is registered for the ferrite powder during milling for 30 minutes of the milling, while crystallite size is declaratively reduced all up to 60 minutes.

A small increase in the crystallite size after 120 minutes, as well as lattice parameters, are for the ferrite powder suggesting competition between recrystallization process and milling induced deformation. Microstrain broadening is showing that deformation mechanisms are dominant up to 60 minutes of milling time, after what the before mentioned recrystallization process is evident. The iron oxide phase does not show a significant increase in crystallite size, but the distortion trends of the lattice *a* and *c* parameters mutually exchange. Strain follows behavior for the majority spinel phase. It is indicative that lattice size parameters of the ferrite and iron oxide phases are during milling in opposite trends. Lattice parameters of the main phase are diminishing while the iron oxide phase is rising. The iron phase in the quantity of 7 % is added to establish a continual surplus of iron. Otherwise, ferrite formation can be missed. Graphically represented data are shown on Fig. 2.

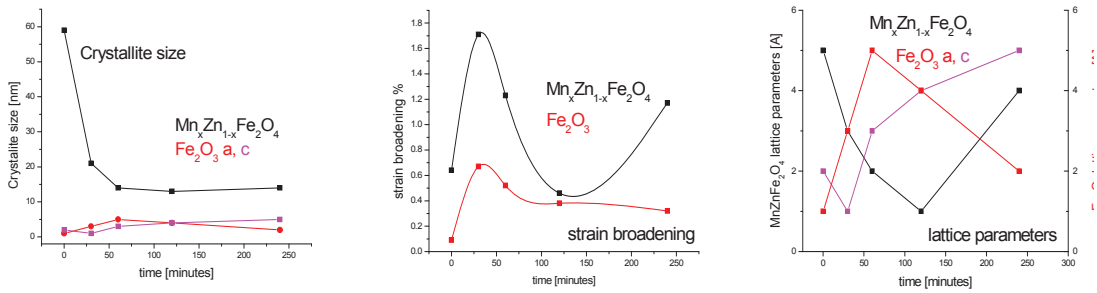

Fig. 2. Crystallite size, strain broadening and lattice parameters for powders milled 30, 60, 120 and 240 minutes obtained from XRD patterns refinement.

The average size and particle size distribution in a water powder suspension were determined by laser particle size analyzer with previous treatment in an ultrasonic bath for 5 min, presented on Fig. 3.

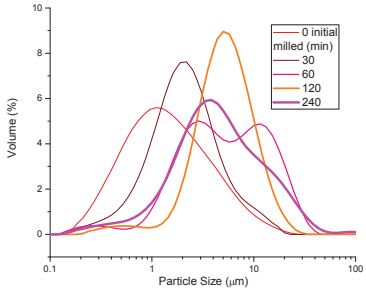

Fig. 3. Particle size distributions for the powders milled 30, 60, 120 and 240 minutes.

The initial powder consisted of average particles of 2.390 μm with a wide span of 3.501 μm. Non activated powder particle size distribution is bimodal. Namely, besides particles about 0.2 microns the asymmetric shape indicates that the powder is initially already agglomerated. Further milling treatment shifts particle size distributions to larger particle sizes. We consider particle breaking process as finished before the first, 30 minutes, milling time observed. After 30 minutes of activation, although SEM micrographs show small particles and XRD analysis decrease in crystallite size, agglomeration of powders leads to the increase of the measured particle size, and the span is slightly smaller. For the powders 60 and 240 minutes, bimodality becomes significant. Those bimodality cycles are representing subsequent processes of secondary agglomeration and recrystallization. When the process of secondary agglomeration is finished recrystallization forms new phase which is then broken again. Two different size fractions can be rudely estimated as 3 and 11 microns in size. Further mechanical activation is repeating monomodal and bimodal distribution. Monomodal 120 minutes reduces the span and the particle size distribution is again mono bimodal due to recrystallization dominancy at this point, but activation time of 240 minutes increases the span again and the particle size distribution is returning to bimodal. In mechanochemistry usual events are finished until 120 minutes, and here that time is doubled, so we consider that the system is repeating processes.

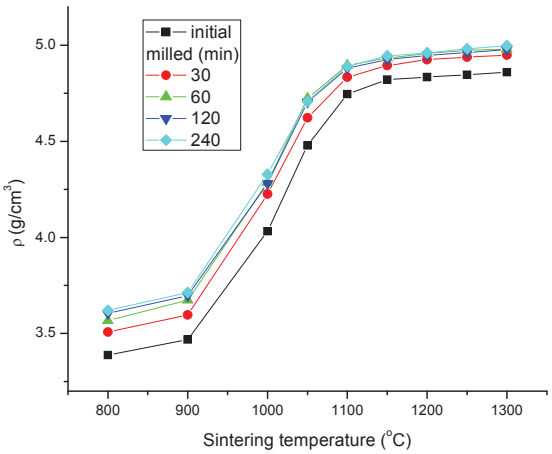

Fig. 4. The density of the sintered specimens obtained from the powders milled 30, 60, 120 and 240 minutes as a function of the sintering temperature.

Green disc samples were sintered in air atmosphere within the temperature interval from 800°C up to 1300°C during 2 hours to explore milling influence on sintering, as well as to exclude melting processes that can influence sintering. Sample density was determined and it was increasing with the sintering temperature up to 1100°C, while after that temperature density increased as well but much slower. Milling procedure has evidently increased sintered sample density, but milling longer than 60 minutes did not have a significant influence on the sample density. This is caused by the reduction of the powder`s particle size as well as by the introduction of defects in the solid state structure that is promoting sintering.

Thermal analysis was observed in an air atmosphere. Sintering phenomenon is present as the largest shrinkage event on the diagram at 1000°C. Sintering of Mn-Zn ferrites in air leads to their decomposition at about 700°C, equation 1. Most frequently oxygen atmosphere is changed during heating with nitrogen one up to the temperature where Mn-Zn ferrites become stable. High-temperature region TGA analysis shows a major weight loss event at about 900°C as a loss of oxygen due to the repeated formation of $MnZnFe_2O_4$. Thus remaining manganese ions are reduced from the Mn^{3+} to the Mn^{2+} oxidation state. Oxidation of Mn^{2+} ions is known to proceed most rapidly at 900-1000°C, while the optimal temperature to produce Mn-Zn ferrites lies in the temperature range of 1000°C to 1200°C. Specific cooling

modes, including oxygen control in the furnace chamber, are typically applied to avoid Mn^{2+} oxidation and to produce ferrites with proper functional features [13]. In air atmosphere reformation of Mn-Zn ferrites is followed by oxygen release and expansion noted on the dilatometric device for the powders activated 30 and 60 minutes that originates from an abrupt oxygen release at 1300°C. The combination of milling and sintering conditions is leading to the shortening of diffusion paths and oxygen release hindering that results in swelling of the particular specimens.

$$2Mn_{0.5}Zn_{0.5}Fe_2O_4 + \frac{1}{4}O_2 \Leftrightarrow Fe_2O_3 + \frac{1}{2}Mn_2O_3 + ZnFe_2O_4 \quad (1)$$

During heating of already formed Mn-Zn ferrites, at low temperatures, numerous events are present and thermal characterization methods are extremely important. A spinel configuration is regarded as inverse due to occupancy of the octahedral and tetrahedral sites. Differential thermal gravimetry is indicating oxidation of the specific species at specific temperatures according to their lattice position [14]. Dilatometry is also indicating an oxidation event and thus confirming DTA/TGA analysis. In this case, the events during heating can be divided into three regions. Region I with the weight gain events spread until 400°C. This region is fulfilled with ferrite species oxidation and is very often masked with a binder or reactant residuals release [15]. In this region, we have total oxidation of Fe^{2+} at 200°C for the B octahedral sites position. The following event is also total oxidation of Mn^{3+}at about 270°C, on B sites. Subsequently, follows incomplete oxidation of Mn^{2+} to Mn^{3+}at about 350°C on tetrahedral A sites. All these oxidation events are recognized as a mass gain. At 400°C region I ended and region II starts. Mass loss is present in region II up to 550°C and reduction of Mn^{4+} to Mn^{3+} happens. Above 550°C, region III starts. Here weight gain is originating from the oxidation of Mn^{2+} that were not completely oxidized, and here the phase change is simultaneous from a spinel to a corundum structure [16].

We have employed thermal techniques that can mutually confirm the presence of a particular event with the means of changes in the specimen`s weight, heat transfer, and dimensions. By adopting the before mentioned sequence of events, we can declare changes that have been made due to milling treatment of Mn-Zn ferrite powders. DTG diagrams and derivatives of shrinkage as a function of temperature for the non-activated powder as well as for the activated powders have been presented in figures 5 to 9.

The milling procedure has diminished the oxidation process of Fe^{2+} at 200°C for B sites according to the DTG diagram. The lack of the expansion peak on the shrinkage derivative diagram favors this statement. The DTA diagram is showing a 220°C exothermal peak that is at higher temperatures for the non-activated powder and lowers in position until 60 minutes. During the course of milling, the enthalpy of the process is lowering. We presume that iron oxidation is probably induced during mechanical milling.

This can also be the case for Mn^{3+} total oxidation at 290°C. Here according to the DTG diagram at 290°C, the non-activated sample has a mass reduction, while milled specimens show a little gain. Milling has reduced Mn and the reaction left was a small oxidation gain in Mn^{2+} ions for oxidation after milling. Shrinkage phenomenon is evident for the reduction at 290°C since it is absent for the milled powder. The further 360°C event is partial oxidation of Mn^{2+} to Mn^{3+} for A sites which is highly present for the milled powder. Non-treated powder does not have this event. Here it is worth noting that certain authors indicate manganese segregation near pores due to the Kirkendale effect. Since it is a diffusion phenomenon, the milling procedure has equaled concentrations explaining the difference between the starting powder and the milled one [10].

The mass loss that is most intensive occurs at 580°C and represents a reduction of Mn^{4+} to Mn^{3+}. This reduction is completely absent in the starting powder. On the dilatometric device, it is evidenced as expansion and for non-activated powder as shrinkage. DTA analysis shows an endothermic peak at 570°C for all activated powders.

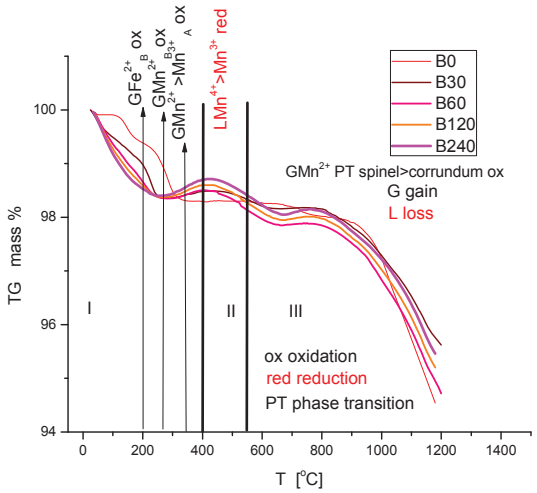

Fig. 5. Thermogravimetric diagram during heating with characteristic temperature regions and events for the powders milled 30, 60, 120 and 240 minutes.

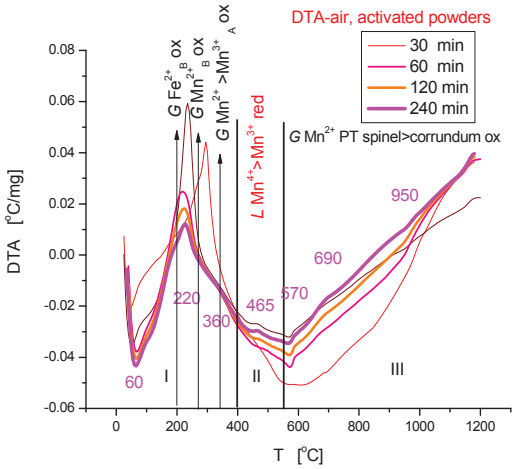

Fig. 6. DTA diagram during heating with characteristic temperature regions and events for the powders milled 30, 60, 120 and 240 minutes.

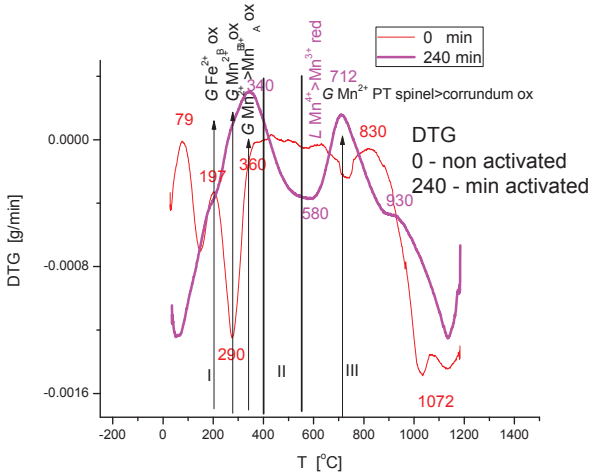

Fig. 7. Characteristic differential of thermal gravimetry for the non-activated powder and 240 minutes activated powder with characteristic temperature regions and events.

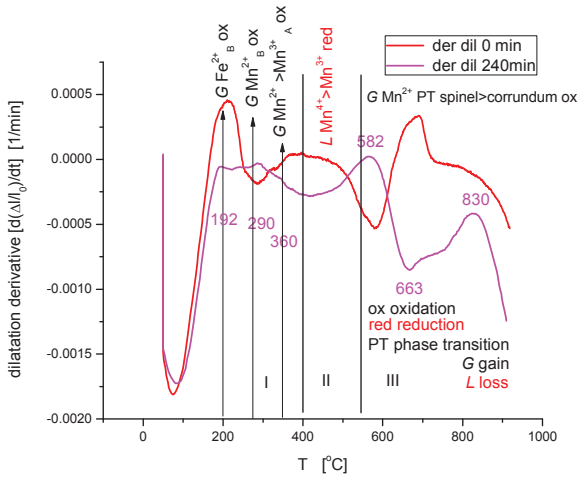

Fig. 8. Shrinkage rate (dilatation derivative) as a function of temperature with characteristic temperature regions and events.

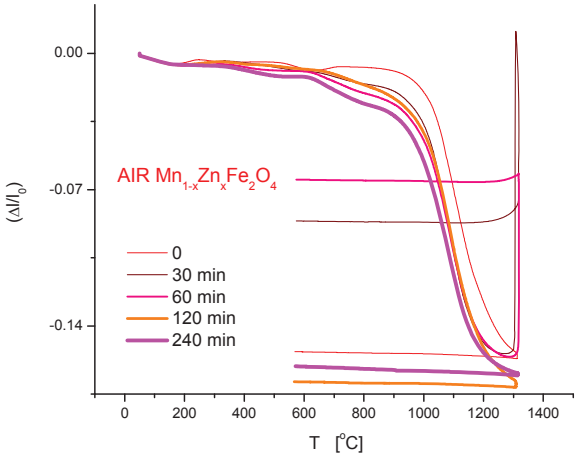

Fig. 9. Shrinkage (dilatograms) for the powders milled 30, 60, 120 and 240 minutes during heating and cooling stages.

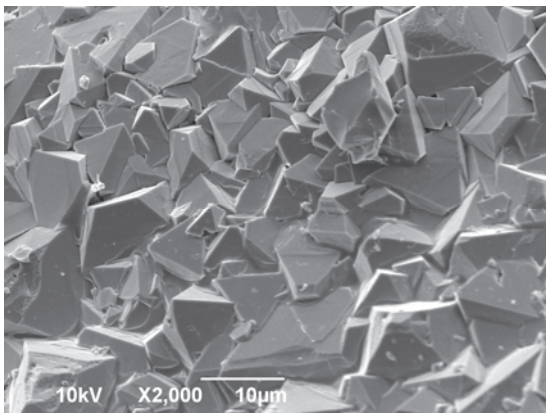

Fig. 10. SEM on the breakage of the sintered sample for the non-activated 0, sint 5 min 1300°C, air, 2000x.

The non-activated powder when sintered has a recognizable grain structure, Fig. 10. The micrograph was recorded on a fresh breakage and represents inter-granular fracture. The

grain size is determined from the presented micrographics by rude approximation with the Semafore software ver. 5.2 [17]. The center of the Gauss distribution function is at 0.67 microns and width 0.41 microns. The mean average is 0.77 microns and standard deviation 0.28. Here it is expected that grains have grown uninhibitedly and simultaneously. No porosity was observed.

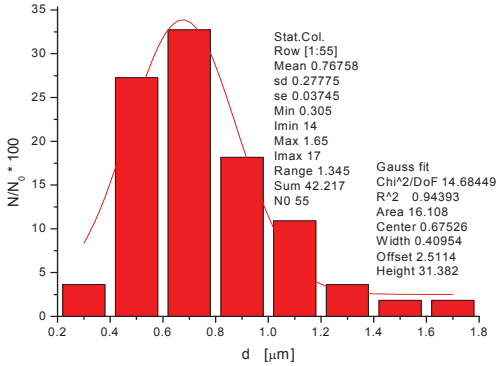

Fig. 11. Grain size distribution for the sintered sample of the non-activated sample.

With mechanical treatment of 30 minutes, intergranular fracture disappears and obviously large grains are now fractured through grains as shown in Figure 12. The grain size cannot be identified in this case since grains boundaries are not representative and distinguishable. Intergranular porosity is noticed with a specific and characteristic irregular shape of pores.

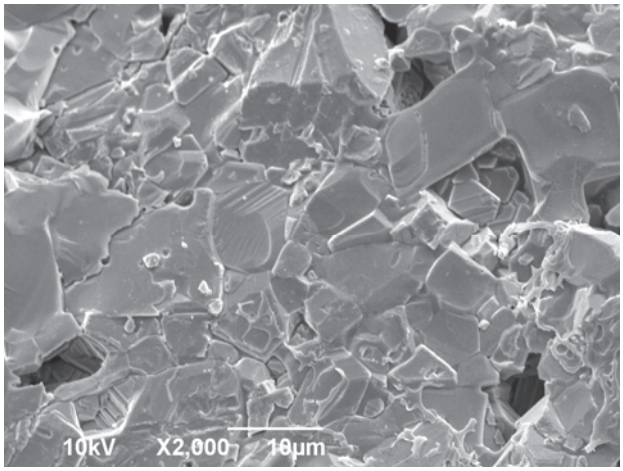

Fig. 12. SEM on the breakage of the sintered sample (starting powder milled for 30 minutes, sint 5 min 1300^{o}C, air), 2000x.

Breakage is also showing specific features characteristic for brittle materials. Since grains are enlarged compared to the non-activated powder, their size enables mutual interfering of fracture surface features such as mirror, mist and hackle periods due to macroscopic crack branching boundaries [18].

One hour activated and sintered samples are showing a higher portion of closed porosity, Figure 13. The rounded pore shape is indicating that specimen defects concentrations enable unpinning of pores from the grain boundaries during grain growth. The formed pores are showing a rounded shape. Closed pores in the interior of the grain can be the product of pore unpinning during grain growth during sintering, or Kirkendalle pores formed

due to the difference in the diffusivity constant difference between vacancies and cations. This is so since oxygen vacancies are considered to be the slowest moving species. It also includes the absence of intergranular pores with a polygonal shape. Grains are larger and definitely distinguishable. Also, there is some possibility that release of oxygen during reduction forms pores, but a deterioration process is more expected. This means that one hour of activation enhances diffusion. But a similar relative expansion on this specimen is showing a dimensional change from -15.5 % to -6.18 % of dilatation in the temperature range from 1262^{o}C to 1317^{o}C. Now, this event is positioned with the same beginning temperature but for this sample prolonged to the beginning of the cooling stage. If we subscribe dilatation to the reaction, which is now possible, since the temperature interval is the same, then the prolonged period leads to the conclusion that different microstructures are indicating a difference in the starting defects.

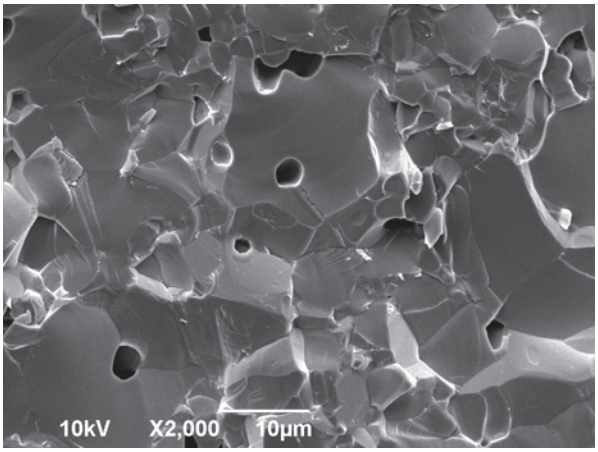

Fig. 13. SEM on the breakage of the sintered sample (starting powder milled for 60 minutes, sint 5 min 1300^{o}C), air, 2000x.

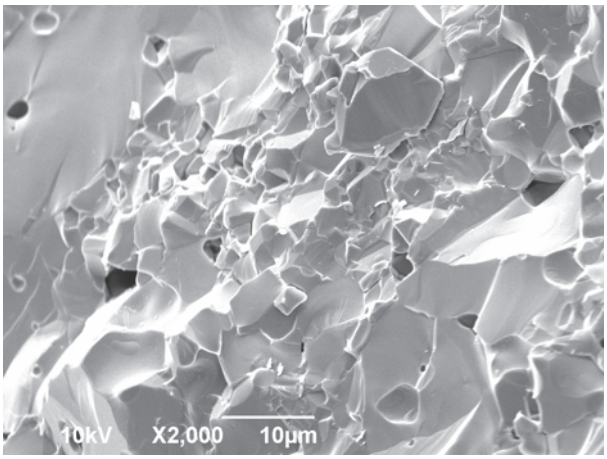

Fig. 14. SEM on the breakage of the sintered sample (starting powder milled for 120 minutes, sint 5 min 1300^{o}C, air), 2000x.

The sample where the starting powder was activated for 2 hours shows well-defined grains, but the almost total absence of porosity, figure 14. Some small examples of closed porosity and a few triple junction small pores can be noted. Dilatogram diagrams show no expansion due to oxygen release. It is possible that due to prolonged milling that reaction is minimized.

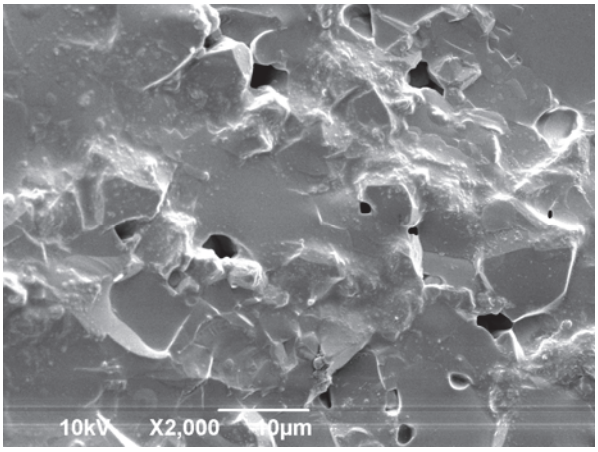

Fig. 15. SEM on the breakage of the sintered sample (starting powder milled for 240 minutes, sint 5 min 1300^{o}C, air), 2000x.

Four hours of milling according to mechanochemistry represents a very long time, figure 15. For this specimen, we noted minimal closed porosity and no grains visible.

4. Conclusion

Milling has completely changed the structure of the original powder since microstructures of the milled powders showed changes in specimens during second heating. Expectations of these preliminary investigations were to find particular sintering conditions that give the desired microstructure such as grain size and porosity and agglomeration of the sinter and milled powders. This goal is hard to achieve since a more detailed investigation needs to be performed due to the complexity of the two preparatory techniques involved such as milling and heating. Also, a complex system does not lead to simplified kinetics but to complex multi-component and phase interactions. In this case for the particular powders and particular synthetic conditions, characteristic oxidation and reduction temperatures of particular cations are revealed as well as following microstructure connections.

Acknowledgement

This work was supported by the Ministry of Science, Education and Technological Development of the Republic of Serbia, projects OI172057 and III45014. We would also like to express our gratitude for useful suggestions to Vladimir Blagojević over the DTG interpretation.

5. References

1. R. Dieckmann, Point defects and transport in non-stoichiometric oxides: solved and unsolved problems, J.Phys.Chem.Solids, 59, 4. (1998) 507-525,
2. J. Töpfer, R .Dieckmann, Point defects and deviation from stoichiometry in $(Zn_{x-y/4}Mn_{1-x-3y/4}Fe_{2+y})_{1-\delta/3}O_4$, Journal of the European Ceramic Society, 24 (2004) 603-612.

3. J.-H. Lee, M. Martin, H.-I.Yoo, Self and impurity cation diffusion in manganese - zinc - ferrite, $Mn_{1-x-y}Zn_xFe_{2+y}O_4$, Journal of Physics and Chemistry of Solids, 61 (2000) 1597-1605.
4. H. Inaba, T. Matsui, Vaporization and Diffusion of Manganese - Zinc Ferrite, Journal of Solid State Chemistry, 121 (1996) 143-148.
5. M. Zdujić, Č. Jovalekić, Lj. Karanović, M. Mitrić, D. Poleti, D. Skala, Mechanochemical treatment of α - Fe_2O_3 powder in air atmosphere, Materials Science and Engineering: A, 245 (1998) 109-117.
6. M. Zdujić, Č. Jovalekić, Lj. Karanović, M. Mitrić, The ball milling induced transformation of α - $Fe2O_3$ powder in air and oxygen atmosphere, Materials Science and Engineering: A, 262 (1999) 204-213.
7. M. Rozman, M. Drofenik, Sintering of Nanosized MnZn Ferrite Powders, Journal of the American Ceramic Socitey, 81, 7 (1998) 1757-1764.
8. E. Ranjithkumar, R. Jayaprakash, M. S. Seehra, T. Prakash, S. Kumar, Effect of α - Fe_2O_3 phase on structural, magnetic and dielectric properties of MnZn ferrite nanoparticles, Journal of Physics and Chemsitry of Solids, 74 (2013) 943 -949.
9. B. S. Zlatkov, N. S. Mitrović, A. M. Maričić, H. Danninger, O. S. Aleksić, E. Halwax, Properties of MnZn ferrites prepared by powder injection molding technology, Materials Science and Engineering B, 175 (2010) 217-222.
10. D. Makovec, M. Drofenik, A. Žnidaršič, Sintering of MnZn-ferrite powders prepared by hydrothermal reactions between oxides, Journal of the European Ceramic Society, 21 (2001) 1945-1949.
11. A. C. Larson, R. B. Von Dreele, General Structure Analysis System (GSAS), Los Alamos National Laboratory Report LAUR (2004) 86-748.
12. B. H. Toby, EXPGUI, a graphical user interface for GSAS, J. Appl. Cryst., 34 (2001) 210-213.
13. D. Kotsikau, M. Ivanovskaya, V. Pankov, Y. Fedotova, Structure and magnetic properties of manganese-zinc-ferrites prepared by spray pyrolysis method, Solid State Sciences, 39 (2015) 69-73.
14. V. Nivoix, P. Perriat, B. Gillot, Modeling of the DTG curves for oxidation of a nanosized molybdenum ferrite coupling mechanics and diffusion, Journal of Thermal Analysis and Calorimetry, 59 (2000) 847-858.
15. R. Mauczok, V. T. Zaspalis, Binder burnout-material - process interaction during sintering of MnZn-ferrites, Journal of European Ceramic Society, 20 (2000) 2121-2127.
16. M. Laarj, I. Pignone, M. el Guendouzi, P. Tailhades, A. Rousset and B. Gillot, Quantitative analysis by derivative thermogravimetry of oxidizable cations for finely divided manganese substituted magnetites, Thermochimica acta, 152 (1989) 187-195.
17. JEOL www. jeol.se ref
18. K. Gopalakrishnana, J. J. Mecholsky, Quantitative fractography of mixed mode fracture in glass and ceramics, Journal of European Ceramic Society, 34 (2014) 3247-3254.

Садржај: *Комерцијални Mn-Zn феритни прах ($Mn_{0.63}Zn_{0.37}Fe_2O_4$, 93 wt.% и Fe_2O_3 7 wt.%) је млевен 0.5, 1, 2 и 4 сата у планетарном млину. Циљ је био посматрање утицаја интензивног мелвења на оксидацију и редукцију која се појављује током грејања као наредног поступка. Прахови су карактерисани рендгенском дифракцијом, сканирајућом електронском микроскопијом СЕМ, уређајем за одређивње величине честица. Накнадно грејање је праћено на термогравиметријској и диференцијалној термалној анализи ТГА/ДТА у атмосфери ваздуха. Након пресовања млевених прахова,*

изведно је синтеровање које је праћено дилатометријски. Синтеровани узорци су карактерисани микроструктурно са СЕМ микроскопијом на свежем прелому. Добијени први извод по температури термогравиметријске криве указује на интензивне промене настале током продуженог млевења које се показују на кинетици оксидације током грејања. Феритни прахови измењени третманом млевења, као и накнадним загревањем су карактерисани да би се дошло до најбољег могућег односа млевења и синтеровања који би требало применити да бисе дошло до жељене структуре.
Кључне речи: *Ферити, млевење, синтеровање, дилатометрија.*